



Chaotic dynamics of size-dependent curvilinear Euler–Bernoulli beam resonators (MEMS) in a stationary thermal field

Anton V. Krysko^{1,2}  | Jan Awrejcewicz³  | Ilya E. Kutepov⁴  |
Vadim A. Krysko⁴ 

¹ Department of Applied Mathematics and Systems Analysis, Saratov State Technical University, 77 Politehnicheskaya Str., Saratov 410054, Russian Federation

² Cybernetic Institute, National Research Tomsk Polytechnic University, 30 Lenin Avenue, Tomsk 634050, Russian Federation

³ Department of Automation, Biomechanics and Mechatronics, Lodz University of Technology, 1/15 Stefanowskiego St., Lodz 90-924, Poland

⁴ Department of Mathematics and Modeling, Saratov State Technical University, 77 Politehnicheskaya Str., Saratov 410054, Russian Federation

Correspondence

Jan Awrejcewicz, Department of Automation, Biomechanics and Mechatronics, Lodz University of Technology, 1/15 Stefanowskiego St., 90-924 Lodz, Poland.
Email: jan.awrejcewicz@p.lodz.pl

Funding information

Russian Foundation for Basic Research, Grant/Award Number: RFBR 20-08-00354

In this work the chaotic dynamics of flexible curvilinear Euler–Bernoulli micro-beams embedded into a stationary temperature field is investigated. The temperature field is modelled based on a the Duhamel–Neumann theory and is free from the restrictions on the temperature field distribution along beam thickness. The von Kármán geometric strain–stress relations are employed. The governing non-linear PDEs are yielded by the Hamilton principle with an account of the modified couple stress theory. The finite dimension problem is truncated to a finite system of nonlinear ODEs using the finite difference method (FDM) and then the Cauchy problem is solved with a help of the Runge–Kutta method. Action of the 2D thermal field is defined by solution to the heat transfer PDE which is also solved by FDM of the second order of accuracy. The so-called charts of vibration regimes (amplitude-frequency planes) are constructed. In particular, novel features of nonlinear (chaotic) dynamics versus the change of the magnitude of the size (length) dependent parameter are reported.

The carried out numerical analysis is supported by the monitoring of frequency power spectra based on the fast Fourier transform (FFT), phase space projections, Poincaré maps and LLEs (largest Lyapunov exponents). We have also analyzed system chaotic dynamics of the classical and size-dependent beam models versus series of values of the two control parameters, i.e. beam curvature and its size-dependent length. Moreover, we have detected and illustrated the novel scenarios of transition form regular to chaotic vibrations of the studied beams, governed by non-linear PDEs.

KEYWORDS

chaos, Euler–Bernoulli micro-beams, Lyapunov exponent, scenario

1 | INTRODUCTION

Micro-electro-mechanical systems (MEMS) including MEMS-sensors, MEMS-accelerometers and MEMS-gyroscopes with the sizes of nanometers/micrometers to 1 mm play an important role in various branches of industry including air-bag sensors, mobile phone applications, scanning probe microscopy, mass and force sensing, electromechanical filters, sensing of pressure, temperature and electromagnetic phenomena, and others. Though the electronic part of the

mentioned systems is satisfactorily resolved, the mechanical modeling of complex vibrational behavior still requires more effort to achieve reliable and validated results.

The reduction of the size of MEMS mechanical systems increases the frequencies of various combined and parametric resonances, which is required to increase their sensitivity as resonators and sensors. On the other hand the construction of MEMS relies on coupling of very small structural members like beams, plates and shells. In many cases the often-used strong reduction to 1-DoF/2-DoF lumped parameter mechanical systems does not allow for reliable fitting of occurred and experimentally validated nonlinear effects including relatively large structural deformations, displacements-dependent excitation, the nonlinear capacitance between parallel electrodes and beam oscillations, nonlinear effects of electrostatic force, etc. In other words, the sensing phenomena exhibit numerous nonlinear effects including bifurcations, chaos, jumps between stable oscillatory states, and so on.

In spite of the mentioned important issue regarding strong order reduction, i.e. transitions from nonlinear PDEs to simple systems of second order ODEs, there is also a challenging theoretical aspect of the modeling of the vibrating micro/nanostructural members with an account of nonclassical higher order approximations to the beams and plates models [1,2]. Assuming that both difficulties have been removed, there are still open problems regarding the size-effects of the MEMS elements [3,4].

Siewe and Hegazy [5] studied chaotic dynamics of a micromechanical resonator under electrostatic forces with a help of the Melnikov function, reduction of the electrostatically induced homoclinic/heteroclinic chaos was illustrated. In addition, different active controllers were applied to suppress the resonator vibrations.

Braghin et al. [6] achieved increasing of the sensibility of the MEMS gyroscope by shifting the resonance peak of the MEMS translating gyroscope toward the highest frequencies. They developed a simple nonlinear lumped parameter model to schematize the gyroscope. Moreover, the semi-analytical integration method was employed for determination of stable/unstable branches of system's response.

Haghighi and Mrkazi [7] employed the Melnikov method and obtained an analytical criterion for homoclinic chaos of a micromechanical resonator. Furthermore, the robust adaptive fuzzy control algorithm was applied to control chaotic vibrations.

Jia et al. [8] analyzed functionally graded material with temperature-dependent thermo-elastic properties of nanobeams with regard to their buckling effects. The minimum total potential energy principle yielded the governing equations with an account of von Kármán geometric nonlinearity and modified couple stress theory. The thermal-mechanical-electrical buckling was analyzed versus the volume fraction profile parameter, dimensionless length scale parameter, ground electrode shape parameter, the applied voltage, and other parameters.

De Martini et al. [9] studied linear/nonlinear tuning of parametrically excited MEMS oscillators. The developed linear tuning scheme was used for rotation of the parametric instability region. Moreover, the developed methodology allowed to achieve a desired MEMS behavior, by using softening, hardening and mixed nonlinearity effects. Furthermore, two oscillators were fabricated and tested in order to validate tuning concept experimentally.

Feng et al. [10] developed very high frequency silicon nanowire electromechanical resonators based on single-crystal silicon nanowires. It was demonstrated that they offered potential for application in resonant sensing, quantum electromechanical systems, and high frequency signal processing.

Husain et al. [11] reported the fabrication and measurement of a platinum nanowire resonator being suitable to achieve required resonant motion.

Sazonova et al. [12] studied the electrical actuation and detection of the guitar-string-like oscillation modes of doubly clamped nanotube oscillators. The fabricated oscillator allowed to transduce very small forces and to widely tuned the resonance frequency.

Scheible et al. [13] detected and analyzed the Ruelle-Takens route to chaos of a nanomechanical resonator. A transition from regular to chaotic resonator vibrations with n frequencies present was traced experimentally.

Zhang et al. [14] demonstrated experimentally how by varying the voltage amplitude of applied electrical signal implied a dramatical change of the first order parametric resonance in a micromechanical oscillator. The observed phenomenon of variation to the tuning of effective cubic stiffness of the oscillator was validated by the first-order perturbation analysis of the derived nonlinear Mathieu equation.

Wang et al. [15] carried out the theoretical and experimental analyses of a bistable MEMS oscillator exhibiting a strange chaotic attractor. Moreover, the authors developed the secure communication schemes based on the synchronized chaos phenomena.

De Martini et al. [16] studied chaotic oscillators of a MEM oscillator governed by the nonlinear Mathieu equation. The numerical simulation results were confirmed by the experimental results.

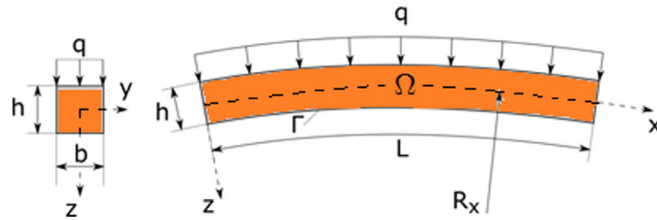


FIGURE 1 Scheme of the studied beam

Aghababa [17] investigated chaotic behavior exhibited by a fractional-order MEM resonator and its suppression. He employed the latest version of the fractional Lyapunov theory, the finite time stability and robustness of the proposed algorithms to study chaotic dynamics of the resonator.

Awrejcewicz et al. [18] formulated mathematical models for deterministic chaos in 1D mechanical continuous systems including various approximations of beam's behaviors. Numerous examples were considered numerically with a help of the so-called charts of the vibrations kind of the investigating mechanical objects with an emphasis put on their chaotic behavior.

Thai et al. [19] carried out a comprehensive review of the state-of-the art of higher-order continuum models for capturing the size effect in small-scale structures. The review included size-dependent analysis of beam, plate and shell models based on the nonlocal elasticity theory, modified couple stress theory and strain gradient theory. Moreover, the research devoted to finite element solutions for size-dependent beam and plate phenomena was presented.

Krysko et al. [20,21] employed the Sheremetev–Pelekh–Reddy–Levinson hypotheses to study the size-dependent static and dynamic behavior of both Bernoulli–Euler and Timoshenko taking into account both geometric and physical nonlinearity. In particular, the influence of the size-dependent coefficient on the load-deflection and stress-strain states of the various beam models were illustrated and analyzed.

Krysko et al. [22] proposed mathematical model and carried out analysis of spatio-temporal chaotic dynamics of flexible simple and curved Euler–Bernoulli beams, taking into account the von Kármán geometric nonlinearity. Time histories, phase and modal portraits, autocorrelation functions, the Poincaré maps, as well as signs of the first four Lyapunov exponents were analyzed. A novel scenario of transition from regular to chaotic dynamics, and from chaos to hyper-chaos were detected and studied.

Based on the so far presented review of the state-of-the art of the research devoted to nonlinear dynamics of the size-dependent structures composed of beams, one may observe that in general chaotic dynamics of size-dependent structural members is less investigated, and in particular with regard to an account of thermal field action. In this work, we are aimed on giving application oriented recipes to predict and control system behavior based on the appropriate choice of the system parameters. In addition, we report various scenario of system transition from regular to chaotic dynamics with regard to both size-dependend parameter and beam curvature.

This paper is organized in the following way. Section 2 presents the used assumptions and hypotheses, and the governing equations. Description of the employed algorithms for the numerical studies are given in Section 3, whereas the numerical case studies are reported in Section 4. The last Section 5 is devoted to conclusions.

2 | HYPOTHESIS AND GOVERNING EQUATIONS

Figure 1 presents the investigated curvilinear beam of length L , height h , its rectangular cross-section of width b and surface A , and its middle line curvature $k_x = 1/R_x$. The beam width is defined from the ratio $b/h = 1$. The mean of boundary occupies the area $\Omega = \{0 \leq x \leq L; -h/2 \leq z \leq h/2\}$.

The beam mathematical model obeys the following hypotheses and assumptions:

- (i) Euler–Bernoulli hypothesis;
- (ii) deformation–displacement geometric nonlinearity is based on the von Kármán assumption;
- (iii) beam sloping obeys the Vlasov condition [23];
- (iv) the beam material is isotropic and the Duhamel–Neumann assumption holds;
- (v) both heat transfer coefficient and beam material physical properties do not depend on temperature;
- (vi) there are not a priori restrictions on the temperature field distribution along the beam thickness.

The governing beam PDEs, boundary and initial conditions are yielded by the energetic Hamilton principle. Namely, a comparison of two neighborhood beam motions in the initial (t_0) and final (t_1) states are considered. In the case of real world beam movement, the following condition must be satisfied

$$\int_{t_0}^{t_1} (\delta K - \delta \Pi + \delta W) dt = 0, \quad (1)$$

where K , kinetic Energy; Π , potential energy; W , sum of elementary works of the external forces.

In the case of isotropic homogenous beam material, the stresses caused by kinematic parameters and intensity of the deformation energy are defined by the following equations

$$\sigma_{ij} = \lambda \varepsilon_{ij} \delta_{ij} + 2\mu \varepsilon_{ij}, \quad m_{ij} = 2\mu l^2 \chi_{ij}, \quad (2)$$

where δ_{ij} stands for the Kronecker symbol; σ_{ij} , ε_{ij} , m_{ij} and χ_{ij} denote components of the classical tensor of stresses σ , deformation tensor ε , the deviatoric part of the symmetric tensor of the higher order moment m and the symmetric part of the curvature χ , respectively; $\lambda = \frac{E\nu}{(1+\nu)(1-2\nu)}$, $\mu = \frac{E}{2(1+\nu)}$ - Lamé parameters; ν - Poisson's coefficient; l - material length parameter (size dependent), and E - Young modulus. Employing the variational computations with regard to the functions u , w , and carrying the integration by parts, the following equations governing beam dynamics are obtained:

$$\left\{ \begin{array}{l} Eh \left(\frac{\partial^2 u}{\partial x^2} - k_x \frac{\partial w}{\partial x} + L_3(w, w) - \frac{\partial N_t}{\partial x} \right) - \frac{\vartheta}{g} h \frac{\partial^2 u}{\partial t^2} = 0, \\ Eh \left\{ -\frac{h^2}{12} \frac{\partial^4 w}{\partial x^4} + k_x \left[\frac{\partial u}{\partial x} - k_x w - \frac{1}{2} \left(\frac{\partial w}{\partial x} \right)^2 - w \frac{\partial^2 w}{\partial x^2} \right] \right. \\ \left. + L_1(u, w) + L_2(w, w) - \frac{\partial^2 M_t}{\partial x^2} - k_x N_t - \frac{\partial}{\partial x} \left\{ N_t \frac{\partial w}{\partial x} \right\} \right\} \\ \left. + q - \frac{\vartheta}{g} h \frac{\partial^2 w}{\partial t^2} - \varepsilon \frac{\vartheta}{g} h \frac{\partial w}{\partial t} = 0, \right. \end{array} \right. \quad (3)$$

where $w(x, t)$, beam element deflection; ε , damping coefficient; $u(x, t)$, beam element displacement; M_x^T , thermal bending moment; N_x^T , longitudinal thermal force; t , time; ϑ , specific beam material weight; g , Earth acceleration; ρ , beam density; q , external load.

The following nondimensional parameters (with bars) are introduced

$$\bar{w} = \frac{w}{h}, \quad \bar{u} = \frac{uL}{h^2}, \quad \bar{x} = \frac{x}{L}, \quad \bar{z} = \frac{z}{h}, \quad \bar{q} = q \frac{L^4}{h^4 E},$$

$$c = \sqrt{\frac{Eg}{\rho}}, \quad \bar{\varepsilon} = \frac{\varepsilon L}{c}, \quad \bar{t} = \frac{t}{\tau}, \quad \tau = \frac{L}{c}, \quad \lambda = \frac{L}{h}, \quad (4)$$

$$\gamma = \frac{l}{h}, \quad \bar{k}_x = \frac{k_x L^2}{h}, \quad \bar{N}_x^T = \frac{N_x^T L^2}{Eh^3}, \quad \bar{M}_x^T = \frac{M_x^T}{Eh^2}, \quad \bar{T} = \alpha T,$$

and the following harmonic external load is employed $q = q_0 \sin(\omega_p t)$, where q_0 stands for the load amplitude and ω_p for its frequency.

After introduction of the introduced dependencies (bars over the nondimensional parameters are omitted), the following counter part of the governing PDEs are obtained

$$\left\{ \begin{array}{l} \frac{\partial^2 u}{\partial x^2} - k_x \frac{\partial w}{\partial x} + \frac{\partial w}{\partial x} \frac{\partial^2 w}{\partial x^2} - \frac{\partial N_x^T}{\partial x} - \frac{\partial^2 u}{\partial t^2} = 0, \\ \frac{1}{\lambda^2} \left\{ \left(-\frac{1}{12} + \frac{l^2}{4} \right) \frac{\partial^4 w}{\partial x^4} + k_x \left[\frac{\partial u}{\partial x} - k_x w - \frac{1}{2} \left(\frac{\partial w}{\partial x} \right)^2 - w \frac{\partial^2 w}{\partial x^2} \right] \right. \\ \left. + \frac{\partial^2 u}{\partial x^2} \frac{\partial w}{\partial x} + \frac{\partial u}{\partial x} \frac{\partial^2 w}{\partial x^2} + \frac{3}{2} \left(\frac{\partial w}{\partial x} \right)^2 \frac{\partial^2 w}{\partial x^2} \right\} - \frac{\partial^2 M_x^T}{\partial x^2} - k_x N_x^T \\ \left. - \frac{\partial}{\partial x} \left\{ N_x^T \frac{\partial w}{\partial x} \right\} + q - \frac{\partial^2 w}{\partial t^2} - \epsilon \frac{\partial w}{\partial t} = 0. \right. \end{array} \right. \quad (5)$$

It should be noticed that when we remove temperature and take $k_x = 0$, PDEs (5) coincide with the PDEs reported in [20], which validates our modeling procedure.

Thermal moments M_x^T and stresses N_x^T appeared in (5) are defined in the following way

$$N_x^T = \int_{-1/2}^{1/2} T(x, z) dz, \quad M_x^T = \int_{-1/2}^{1/2} T(x, z) z dz. \quad (6)$$

As it has been mentioned that there are not any restrictions imposed to the temperature distribution, and the temperature field is defined by a solution to the following heat transfer equation

$$\nabla^2 T(x, z) = \frac{\partial^2 T(x, z)}{\partial x^2} + \lambda^2 \frac{\partial^2 T(x, z)}{\partial z^2} = 0, \quad (7)$$

with the boundary conditions either of the first kind

$$T(x, z)|_{\Gamma} = g_1(x, z), \quad (8)$$

or of the second kind

$$\left. \frac{\partial T(x, z)}{\partial n} \right|_{\Gamma} = g_2(x, z), \quad (9)$$

where $\frac{\partial}{\partial n}$ means differentiation along an external normal to the beam boundary Γ . PDEs (5) require boundary and initial conditions. We employ either

$$w(0, t) = u(0, t) = w'_x(0, t) = 0, \quad w(1, t) = u(1, t) = w'_x(1, t) = 0, \quad (10)$$

or

$$w(0, t) = u(0, t) = M_x(0, t) = 0, \quad w(1, t) = u(1, t) = M_x(1, t) = 0, \quad (11)$$

and the following initial conditions are taken

$$w(x, 0) = f_1(x), \quad \dot{w}(x, 0) = f_2(x), \quad u(x, 0) = f_3(x), \quad \dot{u}(x, 0) = f_4(x). \quad (12)$$

3 | ALGORITHMS

It should be mentioned that numerous researchers dealing with nonlinear dynamics of structural members (non-linear PDEs) employ strong reduced order modeling where often the problem is reduced to either one or two

TABLE 1 Boundary conditions employed to heat transfer PDE

	Boundary condition			View of beam temperature distribution
Kind I	$T(x, z) = g_1(x, z)$	$z = -1/2$	$0 < x < 1$	
	$T(x, z) = 0$	$z = 1/2$	$0 < x < 1$	
	$T(x, z) = 0$	$x = 1$	$-1/2 < z < 1/2$	
	$T(x, z) = 0$	$x = 0$	$-1/2 < z < 1/2$	

Duffing-type ODEs. On contrary, in our work we consider more general approach, i.e. we consider problem with almost infinite dimension.

Namely, we are aimed on application of the FDM of the second order accuracy [22]. For this purpose, the beam space is substituted by the uniform grid (mesh) with the number of nodes $n = 80$. The partial derivatives are substituted by the central finite-difference, through the following approximations

$$\begin{aligned}\Lambda_x(\cdot)_i &= \frac{(\cdot)_{i+1} - (\cdot)_{i-1}}{2\Delta x}, & \Lambda_{x^2}(\cdot)_i &= \frac{(\cdot)_{i+1} - 2(\cdot)_i + (\cdot)_{i-1}}{\Delta x^2}, \\ \Lambda_{x^4}(\cdot)_i &= \frac{(\cdot)_{i+2} - (\cdot)_{i+1} + 6(\cdot)_i - (\cdot)_{i-1} + (\cdot)_{i-2}}{\Delta x^4}.\end{aligned}\quad (13)$$

Finally, the problem is reduced to the following counter-part nonlinear ODEs

$$\begin{aligned}\ddot{u} &= \Lambda_{x^2}(u_i) - \Lambda_x(w)_i \Lambda_{x^2}(w)_i - \Lambda_x(N_x^T)_i, \\ \ddot{w} + \varepsilon \dot{w} &= \frac{1}{\lambda^2} \left\{ \left(-\frac{1}{12} + \frac{l^2}{4} \right) \Lambda_{x^4}(w)_i + k_x \left[\Lambda_x(u_i) - k_x w_i - \frac{1}{2} (\Lambda_x(w)_i)^2 - w_i \Lambda_{x^2}(w)_i \right] \right. \\ &\quad \left. + \Lambda_{x^2}(u)_i \Lambda_x(w)_i + \Lambda_x(u)_i \Lambda_{x^2}(w)_i + \frac{3}{2} (\Lambda_x(w)_i)^2 \right. \\ &\quad \left. \Lambda_{x^2}(w)_i \right\} + k_x (N_x^T)_i - \Lambda_{x^2}(M_x^T)_i - \Lambda_x(N_x^T)_i \Lambda_x(w)_i - \Lambda_x(N_x^T)_i \Lambda_{x^2}(w)_i + q.\end{aligned}\quad (14)$$

The FDM is also employed to the boundary conditions (10)-(11) as well as to the initial conditions (12). The nondimensional PDEs (bars are omitted) (14) are solved by using the Runge–Kutta methods of the 4th and 6th order. The carried-out case studies of computations showed that the results obtained through both methods coincide, and hence we have further used the 4th order Runge–Kutta algorithm due to its efficiency [18].

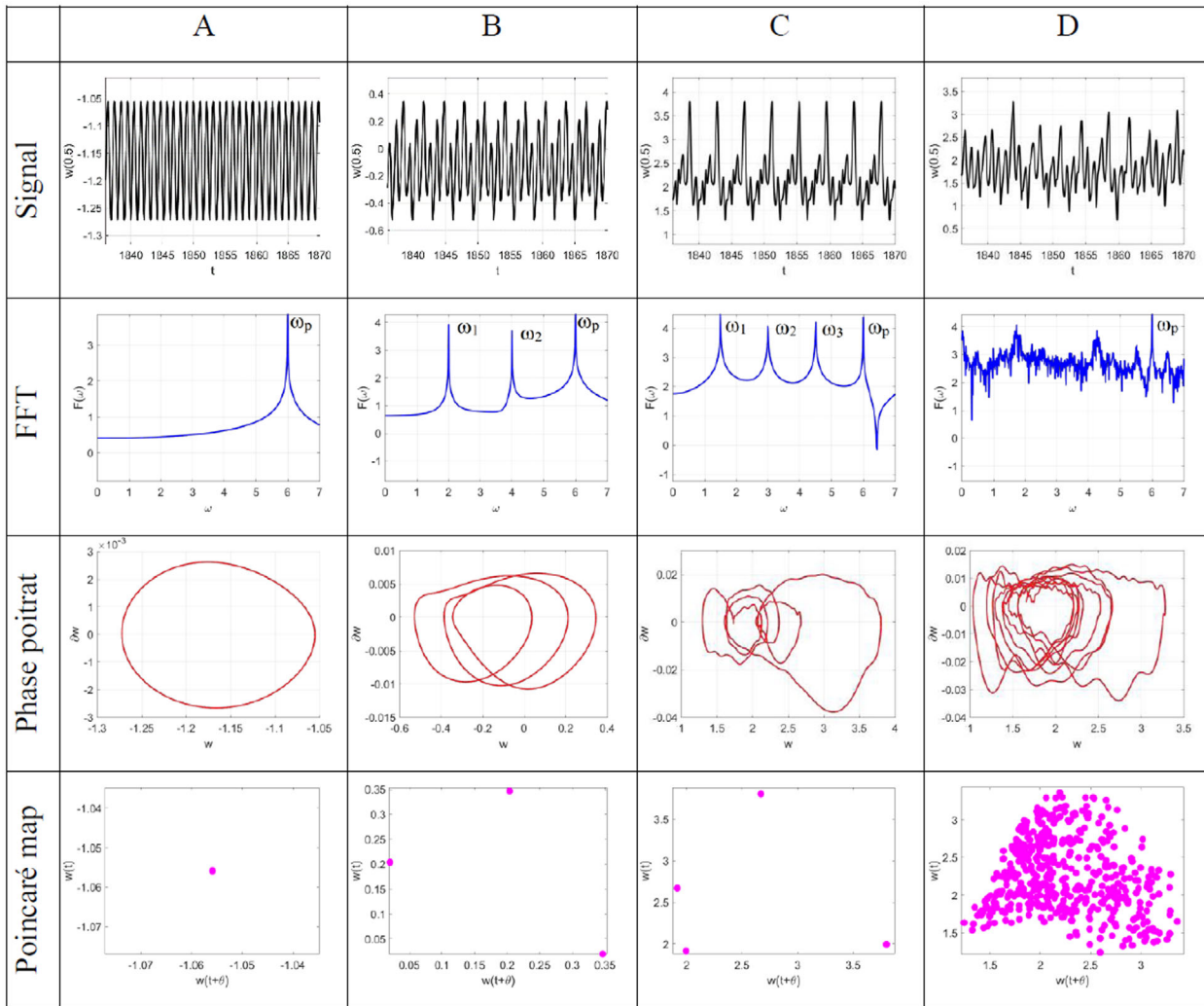
The heat transfer PDE (7) is also solved using FDM (it is already well known and hence not discussed here). In the latter case the most optimal grid resolution stands for 10×80 . The choice has been validated with the analytical solution obtained by Carslaw and Jaeger [24] for the case of the boundary condition of the first kind. The estimations of M_x^T and N_x^T through formulas (6) are carried out with a help of the Simpson method. We have employed standard approaches during computations like removal of the points of conjunction, increase (decrease) of the nodes numbers of the nonregular (regular) grid, etc.

We have also taken into account compatibility conditions while changing boundaries conditions for the case of heat transfer equation, which are reported and considered in [25].

4 | NUMERICAL EXPERIMENTS

Combination of temperature conditions (8)–(9) on the beam's boundaries Γ allow to study various cases of temperature action. In this work we consider temperature field of the first kind presented in Table 1, where also temperature field

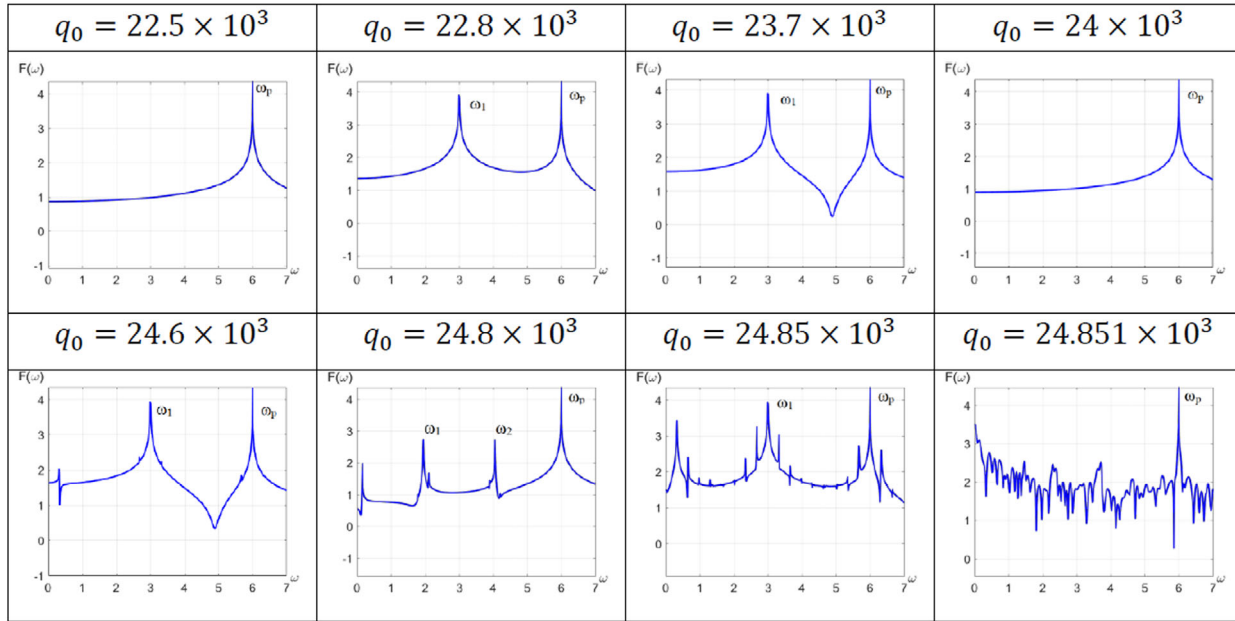
TABLE 2 Beam vibration regimes (more details are given in the text)



distribution is shown. Intensity of the given temperature input T is in the interval $0 \leq T \leq 100^\circ C$. Here and further, the temperature field is given in dimensional form for the case of zinc oxide (ZnO) and in the considered temperature interval of the beam the material characteristics remain unchanged. In order to carry out transition into dimensional temperature values we have used the following fixed parameters: $E = 2.1 \times 10^5$ mPa, $\alpha = 6.5 \times 10^{-6}$ 1/grad and $T = \Delta T + T_0$, $T_0 = 22^\circ C$, where ΔT denotes increment of the temperature $T(x, z)$ defined via the heat transfer PDE (7) subjected to (8).

The following parameters are fixed: $k_x = 12$, $\gamma = 0.5$, $\lambda = 50$, $\varepsilon = 1$, $g_1(x, z) = 50$ (468×10^6 dimensionless units). Table 2 reports the vibrational regimes obtained for $\omega_p = 6$. In the table column A periodic regime is shown, i.e. for $q_0 = 15 \times 10^3$ the signal (time history) exhibits one frequency $\omega_p = 6$, the phase portrait demonstrates stable limit cycle (closed curve) which corresponds to one point of the Poincaré map. Column B of Table 2 ($q_0 = 20.4 \times 10^3$) refers to linear combination of the frequencies (resonances) between three frequencies: $\omega_p = 6$, $\omega_1 = 1/3\omega_p = 2$ and $\omega_2 = 2/3\omega_p = 4$. The phase portrait shows the triple-loop closed curve and the Poincaré map consists of three points. The column C of Table 2 ($q_0 = 43.2 \times 10^3$) is associated with occurrence of two Hopf period doubling bifurcations for the following frequencies amount: $\omega_1 = 1/4\omega_p = 1.5$, $\omega_2 = 2/4\omega_p = 3$, $\omega_3 = 3/4\omega_p = 4.5$ and $\omega_p = 6$. Results shown in column D of the same table ($q_0 = 51.6 \times 10^3$) correspond to chaotic regime where time history is irregular, the frequency spectrum is broad band, and the Poincaré map exhibits chaotic strange attractor.

In order to investigate scenarios of transition of the beam vibrations (from regular to chaotic dynamics) we have monitored FFTs and LLEs for the following fixed parameters: $k_x = 24$, $\lambda = 50$, $\varepsilon = 1$, $g_1(x, z) = 50$ and for the following values of the size-dependent length parameter $\gamma = 0$, $\gamma = 0.3$ and $\gamma = 0.5$. Our investigations are based on the chaos def-

TABLE 3 Transition from regular to chaotic beam vibrations for $\gamma = 0$ and different q_0 based on FFT (Feigenbaum scenario)

initiation given by Gulick [26], where chaotic behavior is defined and recognized by essential system reaction on small changes of initial conditions and the sign of LLEs. We begin with a scenario of transition from regular to chaotic beam vibrations for $\gamma = 0$ (see Table 3). For $q_0 = 22.5 \times 10^3$ we have periodic regime (LEE = -0.00712), and the associated FFT reports one frequency ($\omega_p = 6$). Increase of the excitation amplitude up to the value of $q_0 = 22.8 \times 10^3$ implies birth of $\omega_1 = 1/2\omega_p = 3$, which corresponds to period doubling bifurcation (LEE = -0.00390). The latter state is preserved until the value of $q_0 = 23.7 \times 10^3$. In the interval from $q_0 = 24 \times 10^3$ up to $q_0 = 24.6 \times 10^3$, a zone of periodicity is exhibited (LEE = -0.03372). Further increase of q_0 up to the value $q_0 = 24.8 \times 10^3$ yields occurrence of the resonant frequency $\omega_2 = \omega_p - \omega_1$. For $q_0 = 24.85 \times 10^3$ there are two frequencies (LEE = -0.01127) associated with bifurcation $\omega_1 = 1/2\omega_p = 3$ and linear combination of the frequencies is exhibited. Further increase of q_0 up to $q_0 = 24.851 \times 10^3$ shifts the dynamics beam to chaotic state (LEE = 0.01195). The so far described scenario follows well known Feigenbaum scenario.

Table 4 reports the similar like scenario for $\gamma = 0.3$. For $q_0 = 36.9 \times 10^3$ the beam exhibits periodic vibrations (LEE = -0.03333), and FFT demonstrates the excitation frequency $\omega_p = 6$. Increase of q_0 up to $q_0 = 36.99 \times 10^3$ implies occurrence of the resonance frequency $\omega_2 = \omega_p - \omega_1$ (LEE = -0.00288). Further increase of q_0 generates occurrence of new frequencies (LEE = -0.01320) governed by simple linear relations: $\omega_4 = \omega_p - \omega_3$ for $q_0 = 37.07 \times 10^3$ and $\omega_6 = \omega_p - \omega_5$ for $q_0 = 37.2 \times 10^3$. The mentioned frequencies begin to compete with increase of q_0 shifting the beam vibrations to chaotic regime (LEE = 0.05571). The so far described scenario follows the Ruelle–Takens–Newhouse scenario.

Table 5 reports the beam transition form regular to chaotic vibrations for $\gamma = 0.5$. For $q_0 = 17.1 \times 10^3$ we have periodic vibrations (LEE = -0.00226), with the frequency $\omega_p = 6$. Increase of q_0 up to the value $q_0 = 22.5 \times 10^3$ implies occurrence of three frequencies exhibiting the following subharmonic relations: $\omega_1 = 1/3\omega_p$ and $\omega_2 = 2/3\omega_p$ (LEE = -0.01523). Further increase of the excitation amplitude up to the value of $q_0 = 30.6 \times 10^3$ shifts the system to chaotic vibrations (LEE = 0.01525). The so far scenario follows the previous one, i.e. the Ruelle–Takens–Newhouse scenario.

Therefore, the use of the size-dependent parameter plays a crucial role on the system transition scenario from regular to chaotic motion. The so far discussed and illustrated scenarios are obtained for fixed values of the chosen control parameters. In order to investigate the global system behavior for large intervals of changes of the control parameters $q_0 \in [0; 60 \times 10^3]$ and $\omega_p \in [0; 10]$, the long computations are carried out to define the vibrational regimes of the nano-beams based on the FFT. In result, the charts of nano-beam vibrational regimes versus the values of the amplitude q_0 and frequency ω_p of harmonic excitation are constructed. Each of the charts contains 200×200 pixels (points) which corresponds to getting and analyzing 4×10^4 solutions for a given fixed parameters (q_0, ω_p) (see Figure 2).

TABLE 4 Transition from regular to chaotic beam vibrations for $\gamma = 0.3$ and different q_0 (Ruelle–Takens–Newhouse scenario)

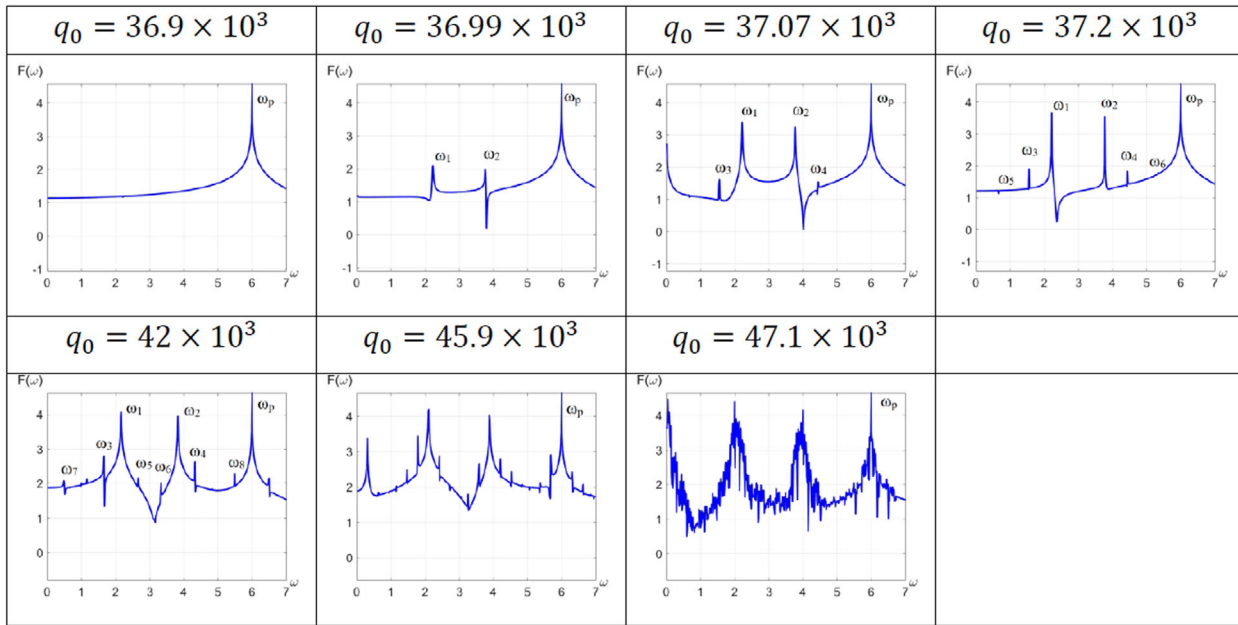


TABLE 5 Transition from regular to chaotic beam vibrations for $\gamma = 0.5$ and different q_0 (Ruelle–Takens–Newhouse scenario)

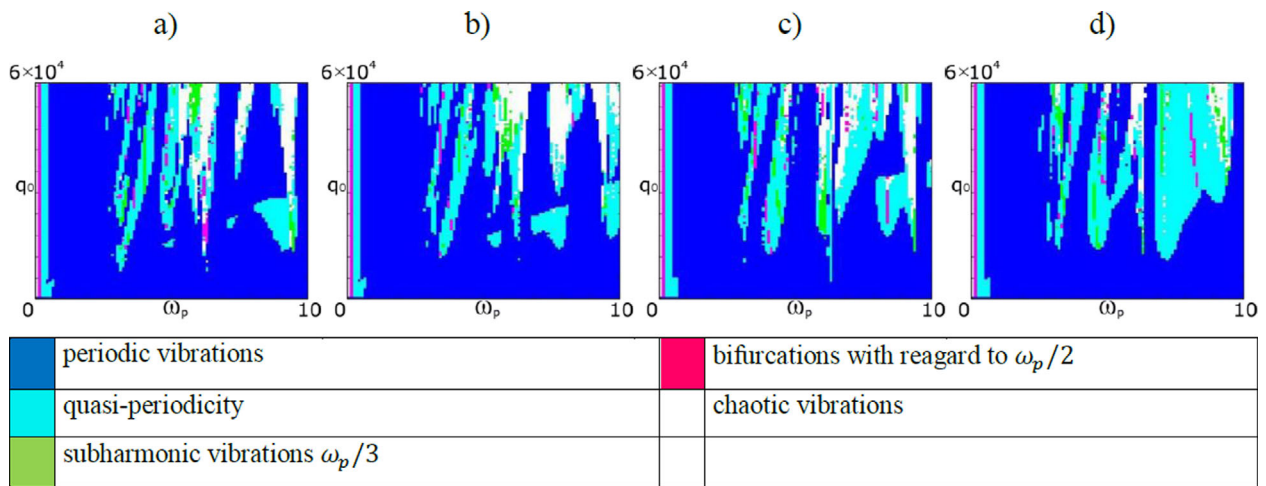
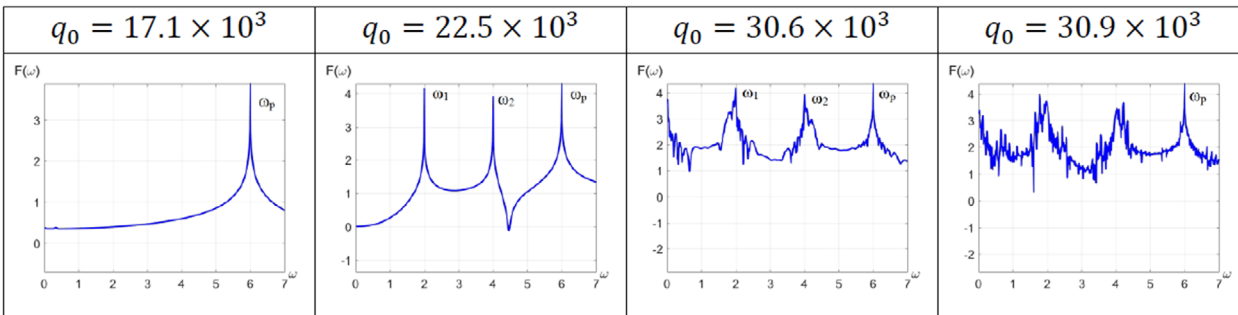


FIGURE 2 Charts of the nano-beam vibration regimes for $k_x = 12$: (a) $\gamma = 0$, (b) $\gamma = 0.3$, (c) $\gamma = 0.5$, (d) $\gamma = 0.7$

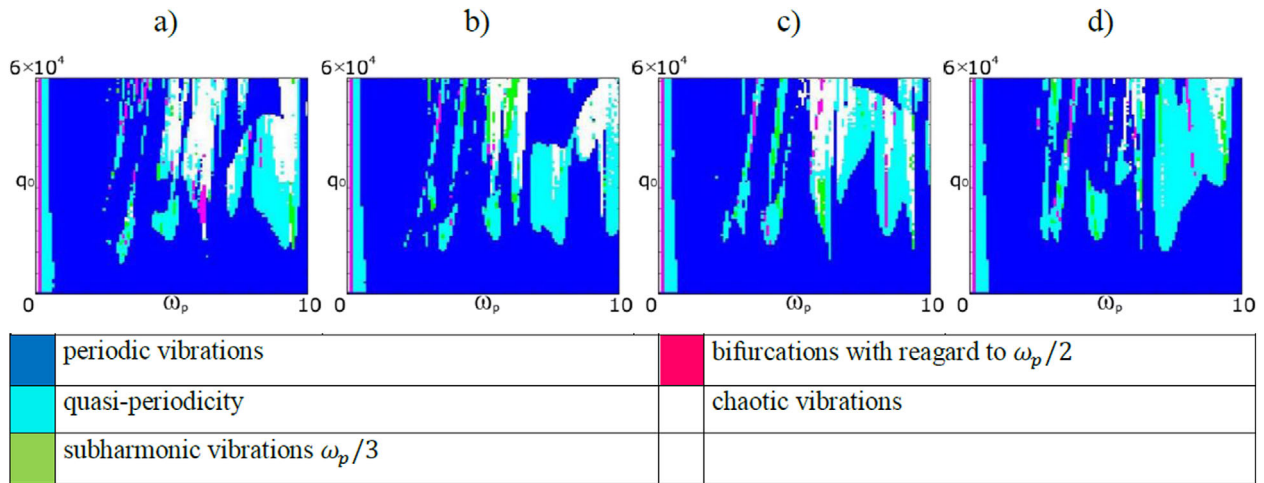


FIGURE 3 Charts of the nano-beam vibration regimes for $k_x = 24$: (a) $\gamma = 0$, (b) $\gamma = 0.3$, (c) $\gamma = 0.5$, (d) $\gamma = 0.7$

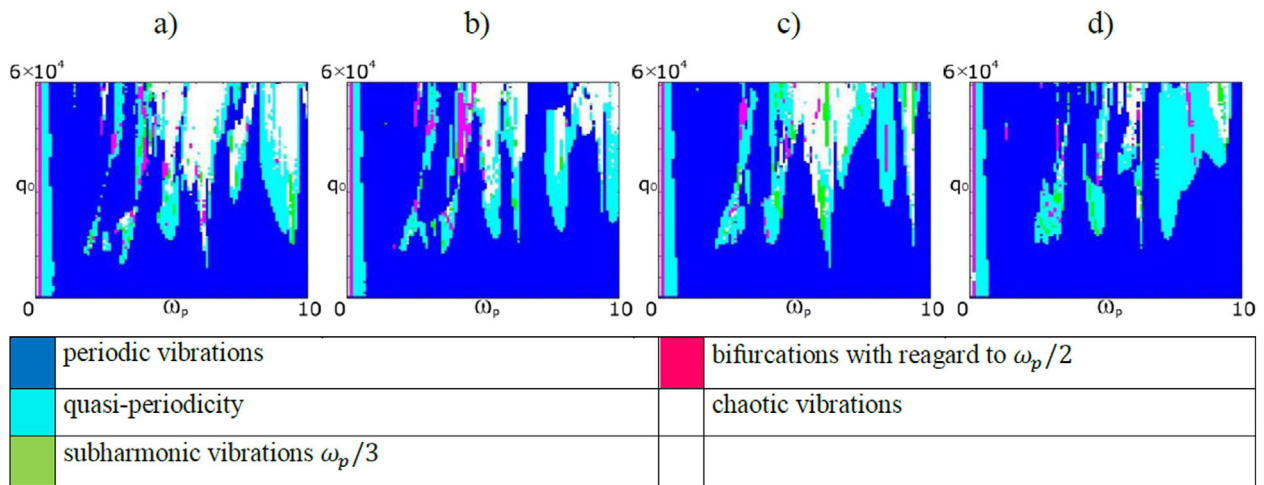


FIGURE 4 Charts of the nano-beam vibration regimes for $k_x = 36$: (a) $\gamma = 0$, (b) $\gamma = 0.3$, (c) $\gamma = 0.5$, (d) $\gamma = 0.7$

Based on analysis of the charts reported for $k_x = 12$ (Figure 2) one may conclude that increase of the scale parameter γ from 0 to 0.7 implies decrease of the chaotic zones located in the neighborhood of average ($3 < \omega_p \leq 6$) and high ($6 < \omega_p \leq 10$) frequencies. For $k_x = 24$ (Figure 3) increase of periodic zone in interval of the average frequencies is observed. Finally, for $k_x = 36$ (Figure 4), the area of chaotic zone is decreased with increase of periodic nano-beam vibrations zone.

In other words, for $k_x = 12$ in the interval of low frequencies ($0 < \omega_p \leq 3$) the periodic regime dominates. Increase of γ yields increase of the nano-beam vibrations spanned on the resonance average and high frequencies. Maximum zone of harmonics takes place for $\gamma = 0.3$. For $k_x = 24$ the chart exhibiting maximum zone of periodic vibrations is obtained for $\gamma = 0.3$. In the case of parameters $k_x = 12$ and $k_x = 24$, the occurrence of subharmonic vibrations with $\omega_p/3$ in the interval of average frequencies is observed.

In order to analyze the constructed charts more deeply, the percentage ratios of a given regime to the whole chart area is shown in Figure 5. It allows to conclude that increase of γ implies decrease of chaotic zone from 7.8% to 4.85% ($k_x = 12$), from 11.47% to 3.8% ($k_x = 24$) and from 14.88% to 4.71% ($k_x = 36$).

Increase of the nano-beam curvature k_x from 12 to 36 yields increase of chaotic zone. Periodic zone decreases with increase of γ for $k_x = 12$ from 68.7% to 61.84%, while for $k_x = 24$ and $k_x = 36$ the increase of periodic zone from 65.38% to 66.28% and from 61.30% to 69.31% is observed, respectively. Finally, the vibration zone spanned on resonance frequencies increases for the all investigated values of the parameter k_x .

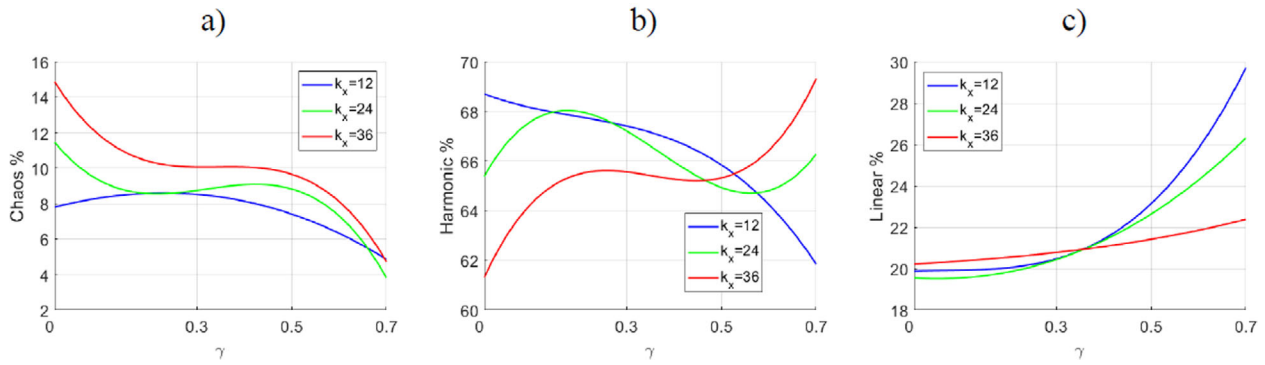


FIGURE 5 Percentage of chaotic (a), periodic (b), and resonance (c) zones versus the size-dependent parameter

5 | CONCLUDING REMARKS

This paper presents a methodology for modeling Euler–Bernoulli microbeams and the temperature field based on the Duhamel–Neumann theory and with an account of the von Kármán geometric nonlinearity. After transition from nonlinear PDEs to a system of coupled nonlinear ODEs with a help of the FDM, the standard numerical approaches have been employed to detect and monitor the nonlinear system effects including scenarios of transition from regular to chaotic microbeam dynamics.

Investigation of chaotic dynamics of the size-dependent flexible beams embedded into temperature field allows to formulate the following main conclusions.

1. Nonlinear dynamics of size-dependent beams essentially depends on the control parameters, i.e. amplitude and frequency of harmonic excitation, the geometric parameter k_x and the scale parameter γ .
2. Scale parameter γ effects transition from regular to chaotic vibrations of the beam. For $\gamma = 0$ the transition follows the Feigenbaum scenario. In the case of $0 < \gamma \leq 0.4$, the modified Ruelle–Takens–Newhouse scenario is exhibited and for $\gamma > 0.4$, the classical Ruelle–Takens–Newhouse scenario is reported.
3. Analysis of the charts of vibrational regimes in the plane $\{q_0; \omega_p; k_x; \gamma\}$ yielded the following observations: (i) increase of curvature k_x of the nano-beams implies decrease of the periodic nano-beam vibrations in a zone of low frequencies; (ii) increase of the scale parameter ($\gamma > 0$) yielded decrease of zone of chaotic vibrations in the interval of high frequencies; (iii) in the case of the nano-beam with $\gamma = 0.3$ and $k_x = 36$ subharmonic vibrations are exhibited with $\omega_p/2$.
4. In the case of classical model ($\gamma = 0$), increase of k_x yielded increase (decrease) of the chaotic (periodic) zone in the interval of high frequencies.
5. Increase of the scale parameter implies decrease of the percentage ratio amount regarding chaotic zone within the interval $0.5 < \gamma \leq 0.7$ independently on the choice of parameter k_x .

ACKNOWLEDGMENTS

This work has been supported by the Russian Foundation for Basic Research RFBR 20-08-00354.

CONFLICT OF INTEREST

The authors declare no potential conflict of interests.

ORCID

Anton V. Krysko  <https://orcid.org/0000-0002-9389-5602>

Jan Awrejcewicz  <https://orcid.org/0000-0003-0387-921X>

Ilya E. Kutepov  <https://orcid.org/0000-0002-1003-4496>

Vadim A. Krysko  <https://orcid.org/0000-0002-4914-764X>

REFERENCES

- [1] Krysko, V.A., Awrejcewicz, J., Zhigalov, M.V., Kirichenko, V.F., Krysko, A.V.: *Mathematical Models of Higher Orders. Shells in Temperature Fields*. Springer, Berlin (2019)

- [2] Awrejcewicz, J., Krysko, V.A.: Elastic and Thermoelastic Problems in Nonlinear Dynamics of Structural Members. Applications of the Bubnov-Galerkin and Finite Difference Methods. Springer, Berlin (2020)
- [3] Awrejcewicz, J., Krysko-jr., V.A., Yakovleva, T.V., Pavlov, S.P., Krysko, V.A.: Nonlinear dynamics of contact interaction of a size-dependent plate supported by a size-dependent beam. *Chaos* 28, 053102 (2018)
- [4] Awrejcewicz, J., Krysko, V.A., Pavlov, S., Zhigalov, M.V., Kalutsky, L.A., Krysko, A.V.: Thermoelastic vibrations of a Timoshenko microbeam based on the modified couple stress theory. *Nonlinear Dyn.* 99, 919 (2020)
- [5] Siewe, S., Hegazy, M., Hegazy, U.H.: Homoclinic bifurcation and chaos control in MEMS resonators. *Appl. Math. Model.* 35(12), 5533 (2011)
- [6] Braghin, F., Resta, F., Leo, E., Spinola, G.: Nonlinear dynamics of vibrating MEMS. *Sens. Actuators, A* 134, 98 (2007)
- [7] Haghghi, H.S., Markazi, A.H.D.: Chaos prediction and control in MEMS resonators. *Commun. Nonlinear Sci. Numer. Simul.* 15, 3091 (2010)
- [8] Jia, X.L., Ke, L.L., Zhong, X.L., Sun, Y., Yang, J., Kitipornchai, S.: Thermal-mechanical-electrical buckling behavior of functionally graded micro-beams based on modified couple stress theory. *Compos. Struct.* 202, 625 (2018)
- [9] De Martini, B.E., Rhoads, J.F., Turner, K.L., Shaw, S.W., Moehlis, J.: Linear and nonlinear tuning of parametrically excited mems oscillators. *J. Microelectromech Syst.* 16, 310 (2017)
- [10] Feng, X.L., He, R., Yang, P., Roukes, M.L.: Very high frequency silicon nanowire electromechanical resonators. *Nano Lett.* 7(7), 1953 (2007).
- [11] Husain, A., Hone, J., Postma, H.W.Ch., Huang, X.M.H., Drake, T., Barbic, M., Scherer, A., Roukes, M.L.: Nanowire-based very-high-frequency electromechanical resonator. *Appl. Phys. Lett.* 83(6), 1240 (2003)
- [12] Sazonova, V., Yaish, Y., Ustunel, H., Roundy, D., Arias, T.A., McEuen, P.L.: A tunable carbon nanotube electromechanical oscillator. *Nature* 431, 284 (2004)
- [13] Scheible, D.V., Erbe, A., Blick, R.H., Corso, G.: Evidence of a nanomechanical resonator being driven into chaotic response via the ruelle-takens route. *Appl. Phys. Lett.* 81, 1884 (2002)
- [14] Zhang, W., Baskaran, R., Turner, K.: Tuning the dynamic behavior of parametric resonance in a micromechanical oscillator. *Appl. Phys. Lett.* 8, 130 (2003)
- [15] Wang, Y.C., Adams, S.G., Thorp, J.S., MacDonald, N.C., Hartwell, P., Bertsch, F.: Chaos in MEMS, parameter estimation and its potential application. *IEEE Trans. Circ. Syst. Fund. Theor. Appl.* 45(10), 1013 (1998)
- [16] DeMartini, B.E., Butterfield, H.E., Moehlis, J., Turner, K.L.: Chaos for a microelectromechanical oscillator governed by the nonlinear Mathieu equation. *J. Microelectromech. Syst.* 16(6), 1314 (2007)
- [17] Aghababa, M.P.: Chaos in a fractional-order micro-electro-mechanical resonator and its suppression. *Chin. Phys. B* 21(10), 100505 (2012)
- [18] Awrejcewicz, J., Krysko, V.A., Papkova, I.V., Krysko, A.V.: *Deterministic Chaos in One-Dimensional Continuous Systems*. World Scientific, Singapore (2016)
- [19] Thai, H.-T., Vo, T.P., Nguyen, T.-K., Kim, S.-E.: A review of continuum mechanics models for size-dependent analysis of beams and plates. *Compos. Struct.* 177, 196 (2017)
- [20] Krysko, A.V., Awrejcewicz, J., Zhigalov, M.V., Pavlov, S.P., Krysko, V.A.: Nonlinear behaviour of different flexible size-dependent beams models based on the modified couple stress theory. Part 1 Governing equations and static analysis of flexible beams. *Int. J. Non-Linear Mech.* 93, 96 (2017)
- [21] Krysko, A.V., Awrejcewicz, J., Zhigalov, M.V., Pavlov, S.P., Krysko, V.A.: Nonlinear behaviour of different flexible size-dependent beams models based on the modified couple stress theory. Part 2. Chaotic dynamics of flexible beams. *Int. J. Non-Linear Mech.* 93, 106 (2017)
- [22] Krysko, A.V., Awrejcewicz, J., Kutepov, I.E., Zagniboroda, N.A., Dobriyan, V., Krysko, V.A.: Chaotic dynamics of flexible Euler-Bernoulli beams. *Chaos* 34(4), 043130 (2014)
- [23] Vlasov, V.Z.: *General Theory for Shells and Its Application in Engineering*. Gostekhizdat Publ., Moscow (1949)
- [24] Carslaw, H., Jaeger, J.: *Conduction of Heat in Solids*. Oxford University Press, Oxford (1959)
- [25] Awrejcewicz, J., Krysko, V.A., Krysko, A.V.: *Thermo-Dynamics of Plates and Shells*. Springer, Berlin (2007)
- [26] Gulick, D.: *Encounters with Chaos*. McGraw-Hill, New York (1992)

How to cite this article: Krysko AV, Awrejcewicz J, Kutepov IE, Krysko VA. Chaotic dynamics of size-dependent curvilinear Euler–Bernoulli beam resonators (MEMS) in a stationary thermal field. *Z Angew Math Mech.* 2020;e202000109. <https://doi.org/10.1002/zamm.202000109>